Deuterium NMR of a pentylcyanobiphenyl liquid crystal confined in a silica aerogel matrix

S. Kralj, G. Lahajnar, A. Zidanšek, N. Vrbančič-Kopač, M. Vilfan, R. Blinc, and M. Kosec
J. Stefan Institute, University of Ljubljana, Jamova 39, 61111 Ljubljana, Slovenia
(Received 10 February 1993)

The temperature dependence of the deuterium NMR line shape was studied in a pentylcyanobiphenyl (5CB) nematic liquid crystal embedded into lecithin-treated and nontreated continuous-pore silica aerogel matrices. In the lecithin-treated matrix the temperature dependence of the NMR absorption spectra of 5CB exhibits a pronounced first-order nematic-isotropic transition, while in the nontreated matrix only a weak discontinuity was found. The observed almost continuous onset of nematic ordering in the latter case appears to be due to the spread of nematic-isotropic-transition temperatures T_{NI} in different aerogel cavities. In the isotropic phase of 5CB a surface ordering effect of the silica aerogel matrix was observed and the surface order parameter was estimated to be $S_0=0.02\pm0.01$. The surface anchoring of the 5CB molecules is much stronger in the case of a nontreated matrix than in the lecithin-treated one.

PACS number(s): 64.70.Md, 76.60.−k

I. INTRODUCTION

The effects of finite size and surface on the bulk properties of condensed-matter systems have been a subject of basic science and applied research for years [1–6]. In this respect liquid-crystalline systems are an important example where orientational and layer ordering properties are strongly influenced by surface interactions. Incorporating liquid crystals into gel networks has led to the discovery of a new type of nematic electro-optic display with significantly enhanced switching properties [7]. Striking finite-size effects were observed [8–10], for instance, in the case of liquid crystals incorporated into the continuous-pore network of a silica aerogel whose porosity could be varied between 0 and 98% by partial densification [11].

Preliminary studies of liquid crystals embedded into the continuous-pore networks of porous glasses and silica aerogels have already been performed using dielectric, light-scattering, and calorimetric methods [8–10]. Aliev and Breganov [8,9] have investigated different nematic liquid crystals immersed in a "macropore" (typical pore radius $R_{\rm cav}$ up to 0.1 μm) and "micropore" ($R_{\rm cav}<0.07$ μm) porous glassy matrix. They found the nematic-isotropic phase-transition temperature T_{NI} shifted towards higher values due to the surface-interaction ordering effect. From the T_{NI} shift observed they estimated the surface anisotropic interaction energy W_0 to be of the order of 10^{-3} J/m^2. The temperature shift is particularly pronounced in the micropore sample and the transition region shows hysteresis behavior. They claim that the observed hysteresis is due to the formation of a smectic polar layer induced by strong surface interactions.

Bellini *et al.* [10] investigated the octylcyanobiphenyl (8CB) liquid crystal immersed in a silica aerogel network of typical pore dimension $R_{\rm cav}\sim0.02$ μm. The observed anomaly in the temperature dependence of the heat capacity indicated the continuous formation of nematic ordering below the bulk T_{NI}. The continuous-transition-region behavior of confined 8CB was also supported by an optical-transparency study showing no noticeable hysteresis phenomena. The optical study further showed that the average nematic orientational order correlation length was comparable to the typical pore diameter. The depression of T_{NI} was accounted for by an impurity effect. They also suggest that the silica aerogel pore walls have a disordering effect.

In view of several open problems concerning orientational order of liquid crystals in an aerogel matrix we decided to perform a deuterium NMR line-shape study on pentylcyanobiphenyl (5CB) nematic liquid crystal (NLC) deuterated on the β position of the alkyl chain immersed in a silica aerogel matrix. This approach was chosen because the nematic alignment strongly influences the resulting NMR absorption spectrum [12,13] $I(\nu)$. If the diffusion rate is slow enough, $I(\nu)$ directly reveals the orientational distribution of nematic molecules within the sample. The NMR method is particularly important for studies of nematic ordering within cavities of the submicrometer range, since this region is not accessible to most other experimental techniques (e.g., polarization-microscope experiments). In particular we wished to study the temperature dependence of the deuterium NMR line-shape pattern near the bulk nematic-isotropic phase transition, with special emphasis on the effect of a normal or lecithin-treated silica aerogel surface on the nematic orientational ordering.

II. EXPERIMENTAL SETUP

The silica aerogel matrix used for our samples was kindly supplied by Dr. Chaput of Ecole Polytechnique (Palaiseau, France). The initial step in preparing the aerogel is sol-gel condensation in acidic medium of a silicon alkoxide, tetraethoxysilane. A small amount of Cr^{3+} ions was added to the polymerization solution as an NMR relaxing agent for the purposes of another experiment [14]. The alkogel, which results from the gelation of this solution, consists of an interconnected network of branched polymers in which solvent molecules are em-

bedded. An aerogel is obtained by evacuating the solvent from the alkogel under hypercritical conditions. In the nontreated sample the nematic liquid crystal 5CB is introduced into the silica aerogel matrix using capillary action. The lecithin coating of the second sample was achieved by previous treatment of the silica aerogel matrix with a 3 wt. % solution of egg-yolk lecithin in ether which enabled penetration of lecithin into the porous network without affecting its structure. Afterwards the ether was evaporated. As in the previous case, the 5CB was introduced into the silica aerogel under vacuum by capillary action. The pore-size distribution for the silica aerogel and a scanning electron micrograph of the silica aerogel matrix of our sample are shown in Figs. 1 and 2, respectively.

Deuteron NMR spectra were recorded at the resonance frequency of 41.463 MHz, using a Bruker SXP spectrometer and a 6.34-T superconducting magnet. A pair of $\pi/2$ pulses with phase cycling was used to obtain the NMR spectra. 1600–10 000 signal accumulations were taken in the low-temperature nematic phase and 160–1600 averages in the high-temperature isotropic phase.

III. THEORETICAL BACKGROUND

A. Effect of confinement on the nematic structure within cavities

The results of Bellini *et al.* [10] reveal that the nematic ordering in different cavities of a continuous-pore silica aerogel network is only weakly correlated. Therefore within a good approximation we can consider this system as being composed of independent cavities. In most cases the nematic ordering [13] within a cavity is sufficiently well described by two parameters: the director field $\mathbf{n}(\mathbf{r})$ oriented along the local average orientation of nematic molecules, and the local orientational order parameter $S(r)=\langle 3\cos^2\theta-1\rangle_t/2$ (with θ representing the angle between the average and instantaneous local orientation of

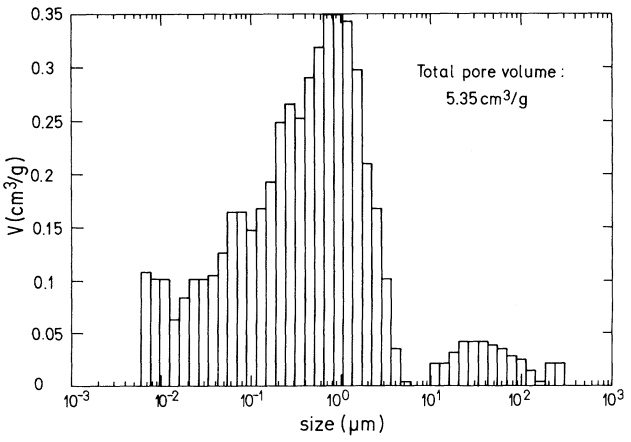

FIG. 1. Pore size distribution for the silica aerogel sample as determined by mercury porosimeter. The height of each column represents the pore volume per gram of aerogel, for pores with sizes indicated by the boundaries of the column.

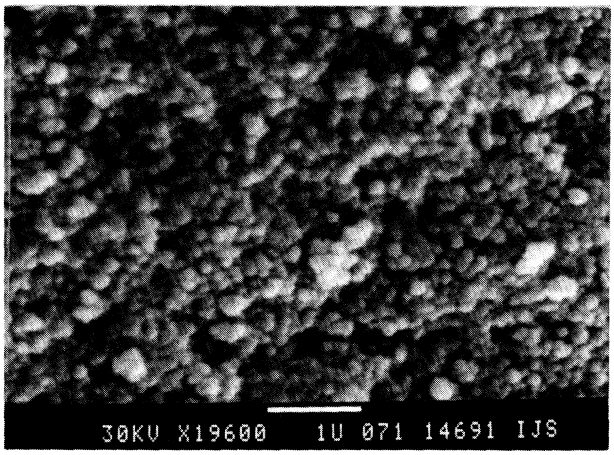

FIG. 2. Scanning electron micrograph of the silica aerogel matrix.

a nematic molecule at a point $\mathbf{r}$, and $\langle\ \rangle_t$ denoting the time average). The $\mathbf{n}(\mathbf{r})$ and $S(\mathbf{r})$ fields depend on the interplay among elastic, surface, and external electric- or magnetic-field interactions. In large cavities [5] ($R_{\rm cav}\geq 0.5$ μm) the $S(\mathbf{r})$ field has an almost constant value through the whole cavity except near the cavity surface and defects.

To evaluate nematic structures within a cavity we start from the Frank [13] nematic free-energy density $f(\mathbf{r})$:

$$f(\mathbf{r})=\frac{K_{11}}{2}(\mathrm{div}\mathbf{n})^2+\frac{K_{22}}{2}(\mathbf{n}\cdot\mathrm{rot}\mathbf{n})^2+\frac{K_{33}}{2}(\mathbf{n}\times\mathrm{rot}\mathbf{n})^2+\frac{W_0}{2}[1-(\mathbf{n}\cdot\mathbf{e}_{\rm easy})^2]\delta(\mathbf{r}-\mathbf{R}_{\rm cav})-\frac{\Delta\chi}{2\mu_0}(\mathbf{n}\cdot\mathbf{B})^2\ . \tag{1}$$

This approach neglects the spatial variation of the orientational order parameter S, which is present in the model via splay (K_{11}), twist (K_{22}), and bend (K_{33}) elastic constants which are in a first approximation proportional to S^2. The nematic phase boundary is designated with the radius vector $\mathbf{R}_{\rm cav}$. W_0 is the surface anchoring strength, which tends to align nematic molecules along the "easy" direction $\mathbf{e}_{\rm easy}$. $\mathbf{B}$ is the external magnetic field and $\Delta\chi$ measures the anisotropy of magnetic susceptibility. The influence of the surface interaction on the nematic structure is represented by the surface extrapolation length d defined as [13]

$$d=K/W_0\ , \tag{1a}$$

where K denotes the average Frank elastic constant. If $\mu=R_{\rm cav}/d\gg 1$ (the so-called strong-anchoring regime), the surface interaction is strong enough to orient nematic molecules along $\mathbf{e}_{\rm easy}$. The influence of the external field on the nematic ordering is measured by the field correlation length [13] ξ. In the case of the external magnetic field it can be expressed as

$$\xi=\sqrt{\mu_0 K/(B^2\Delta\chi)}\ . \tag{1b}$$

In general, the enclosed nematic phase is only weakly influenced by the external magnetic or electric field [15] if $R_{cav}/\xi < 1$.

The minimization of the resulting free energy yields the Euler-Lagrange differential equations which are given in Appendix A. The equilibrium equations are solved numerically using the over-relaxation method. For the sake of simplicity we treat only the case of equal elastic constants $K = K_{11} = K_{22} = K_{33}$. In addition we neglect the external magnetic-field influence (present in the NMR experiment) on the director field assuming that the majority of nematic molecules are within cavities for which $R_{cav}/\xi < 1$ is fulfilled. Since the lecithin coating tends to align nematic molecules homeotropically, and since recent [18] studies indicate that such surface alignment is also realized within the silica aerogel porous matrix, we treat in detail the case of homeotropic anchoring, whereas the tangential case is discussed only briefly.

Recent studies reveal that in the case of homeotropic anchoring in most common cases (cylindrical, spherical cavities) [19–23] radial-like and axial-like structures are obtained (see the nematic structures in Fig. 3). Let us briefly analyze the stability of radial-like and axial-like structures in the case of a weak external magnetic or electric field. The radial-like structures have a larger elastic deformation energy but a lower surface free energy than the axial-like ones. Therefore in cavities, where surface interactions play a dominant role, radial-like structures are preferred [19,20,22]. This is realized in cavities, where $\mu = R_{cav}/d \gg 1$. In smaller cavities ($\mu \ll 1$) the bulk elasticity overwhelms the surface interaction, stabilizing the axial-like structures. The transition between

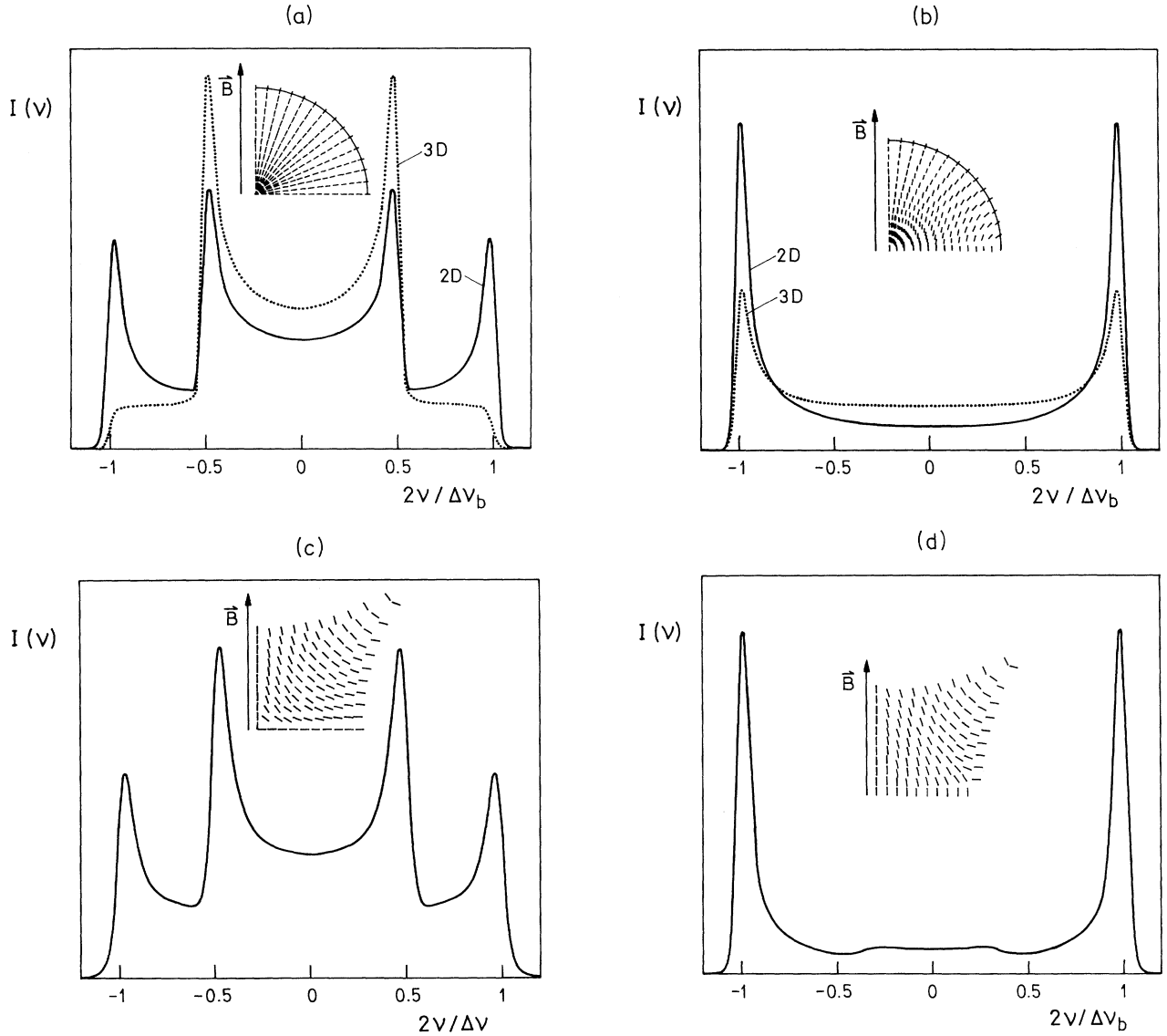

FIG. 3. 2D (a) and (c) radial-like and (b) and (d) axial-like nematic structures within (a) and (b) a spherical cavity and (c) and (d) a cavity of complementary shape, together with the corresponding deuterium absorption spectra for the orientation of **B** as marked in the figure. Structures were numerically evaluated for the case of equal elastic constants. For comparison, the absorption spectra are added (dotted line) for the 3D case of a spherical cavity. In calculations $\delta\nu/\Delta\nu_b$ was set equal to $\frac{1}{30}$.

these competing structures occurs at $\mu=\mu_c$, which in turn defines the critical cavity size $R_c=\mu_c d$ for a fixed value of d. The value of μ_c depends on the cavity shape, the director field within it, and the elastic properties of the NLC. A recent comparative study [20] of such transitions in spherical and cylindrical cavities showed that the qualitative features of the stability diagram of axial-like and radial-like structures realized within these two geometries are preserved and that the values of μ_c are comparable.

B. Deuterium absorption spectrum

Deuterium NMR is an ideal method to probe the structure of a nematic liquid crystal confined to small cavities because the resulting deuterium absorption spectrum $I(\nu)$ strongly depends on the orientational distribution of nematic directors. In the absence of motional averaging, the deuterated nematic molecule located at $\mathbf{r}$ in the cavity contributes two sharp lines to the NMR absorption spectrum separated by [12]

$$\Delta\nu(\mathbf{r})=\frac{S(\mathbf{r})}{S_b}\frac{\Delta\nu_b}{4}[3\cos^2\theta_B(\mathbf{r})-1] \tag{2}$$

where θ_B denotes the angle between the external magnetic field $\mathbf{B}$ and nematic director $\mathbf{n}(\mathbf{r})$, $S(\mathbf{r})$ the orientational order parameter at $\mathbf{r}$, S_b represents the bulk nematic orientational order parameter, and $\Delta\nu_b$ the NMR absorption line splitting of the bulk nematic phase.

If the nematic director is spatially dependent—a case often realized for nematic liquid crystals confined to spatially restricted geometries—the translational diffusion motion induces changes in the orientationally dependent quadrupolar-interaction strength. If the diffusion is fast enough, the resulting spectra may be strongly motionally narrowed. The narrowing due to this mechanism is often called the translationally induced rotation mechanism [16]. It affects considerably the absorption spectra if [15]

$$\epsilon=\Delta\nu_b R_{\rm cav}^2/(6D)\leq 10 \ . \tag{3}$$

Here D stands for an average eigenvalue of the translational diffusion tensor. For typical values of D and $\Delta\nu_b$ (i.e., $D\sim 10^{-11}$ m^2/s and $\Delta\nu_b\sim 10$ kHz), this condition is fulfilled, if the cavity radius $R_{\rm cav}$ is smaller than 0.1 μm.

To calculate a deuterium absorption spectrum $I_{\rm cav}(\nu)$ of the NLC confined into a cavity of typical size $R_{\rm cav}$ we use the expression [12]

$$I_{\rm cav}(\nu)=I_0{\rm Re}\int dt\, e^{-i2\pi\nu t}G(t) \ , \tag{4a}$$

$$G(t)=\left\langle \exp\left[i2\pi\int_0^t\Delta\nu[\mathbf{r}(t')]dt'\right]\right\rangle \ . \tag{4b}$$

$G(t)$ denotes the autocorrelation function and $\langle\ \rangle$ represents an ensemble average. $G(t)$ is evaluated numerically for a given nematic configuration within a cavity using the isotropic random-jump diffusion model [15,17] (see Appendix B).

In general, contributions of different cavities to the NMR absorption spectrum of a sample differ due to the various sizes, shapes, and orientations of the cavities, as well as due to different director distributions within them. The absorption spectra $I(\nu)$ of the whole sample can be then given as

$$I(\nu)=\sum_{\rm cavities}P(R_{\rm cav})I_{\rm cav}(\nu) \ , \tag{5}$$

where $P(R_{\rm cav})$ represents the distribution of nematic molecules over the cavities (see Fig. 1) and the sum runs over all cavities within the sample.

Because of the isotropic character of our silica aerogel sample, it is reasonable to assume that all orientations of $n(\mathbf{r})$ are equally probable if the external magnetic field is weak enough. This is supported by the fact that different orientations of the sample in the external magnetic field gave identical spectra. The corresponding absorption spectrum is expected to be Pake powder shaped of maximum width $\Delta\nu_b$ if surface, pore-size-distribution, and translational-diffusion effects are negligible. Therefore, a departure from this shape clearly indicates the importance of the effects mentioned.

C. Numerical simulations

Individual cavities of a continuous-pore silica aerogel matrix are of different, most probably irregular, shape. To calculate the nematic structure within such cavities and obtain the corresponding absorption spectra $I(\nu)$ would be in general an extremely difficult task. As a first step we analyze the absorption spectra for different nematic structures within two-dimensional (2D) cavities of circular and "complementary" shape [a space between four stacked cylinders; see structures in Figs. 3(c) and 3(d)]. From the results obtained we try to reach some general conclusions which are necessary to understand the behavior of the realistic, 3D sample.

1. Two-dimensional cavities

Figure 3 shows in the inset radial-like and axial-like nematic structures in a (a) and (b) circular and (c) and (d) "complementary" shaped 2D cavity, as well as the corresponding absorption spectra $I(\nu)$ for the case of strong anchoring and without motional narrowing. The results clearly indicate that the modification of the 2D cavity shape from the circular to the complementary ($a\rightarrow c, b\rightarrow d$) relatively weakly affects $I(\nu)$ and that qualitative features of $I(\nu)$ are preserved. $I(\nu)$ of the radial-like structure does not depend (or only weakly) on the orientation of $\mathbf{B}$ in the cavities smaller than the magnetic coherence length. In the case of the axial-like structure $I(\nu)$ remarkably depends on the external field orientation.

The effect of translational diffusion on the corresponding 2D spectra is demonstrated in Fig. 4 for the structures given in Figs. 3(c) and 3(d). It is evident that the radial-like structures are more strongly influenced by translational diffusion than the axial ones.

2. Three-dimensional cavities

In Figs. 3(a) and 3(b) static absorption spectra of a nematic liquid crystal in 3D cavities of spherical shape are superimposed on the spectra of corresponding 2D ax-

ial and radial structures. We see that only $I(\nu)$ of the radial structure is qualitatively changed. In addition, in the case of radial-like structures, the motional averaging induced by translational diffusion can evidently be different in 3D; e.g., in the radial structure $I(\nu)$ can be narrowed into a single line, as is demonstrated in Fig. 5.

Encouraged by these similarities found for cavities of different shapes, our further theoretical considerations were restricted to 3D spherical cavities with the homeotropic boundary condition, for which radial and axial structures are most commonly stable [see the structures in Figs. 3(a) and 3(b)]. In the following we study a sample of dispersed spherical nematic droplets of different radii R_{cav} distributed according to Fig. 1 and calculate a corresponding deuterium NMR absorption spectrum $I(\nu)=\sum P(R_{cav})I_{cav}(\nu)$, taking into account the motional narrowing due to the translational diffusion of nematic molecules. Since cavity dimensions (R_{cav}) are distributed both above and below a critical dimension R_c, where the transition between the axial and radial structure takes place, the resulting spectrum $I(\nu)$ is expected to be composed of the spectral contributions $I_{cav}(\nu)$ of both structures. For this reason let us first make a brief analysis of $I_{cav}(\nu)$ for each of the two structures separately.

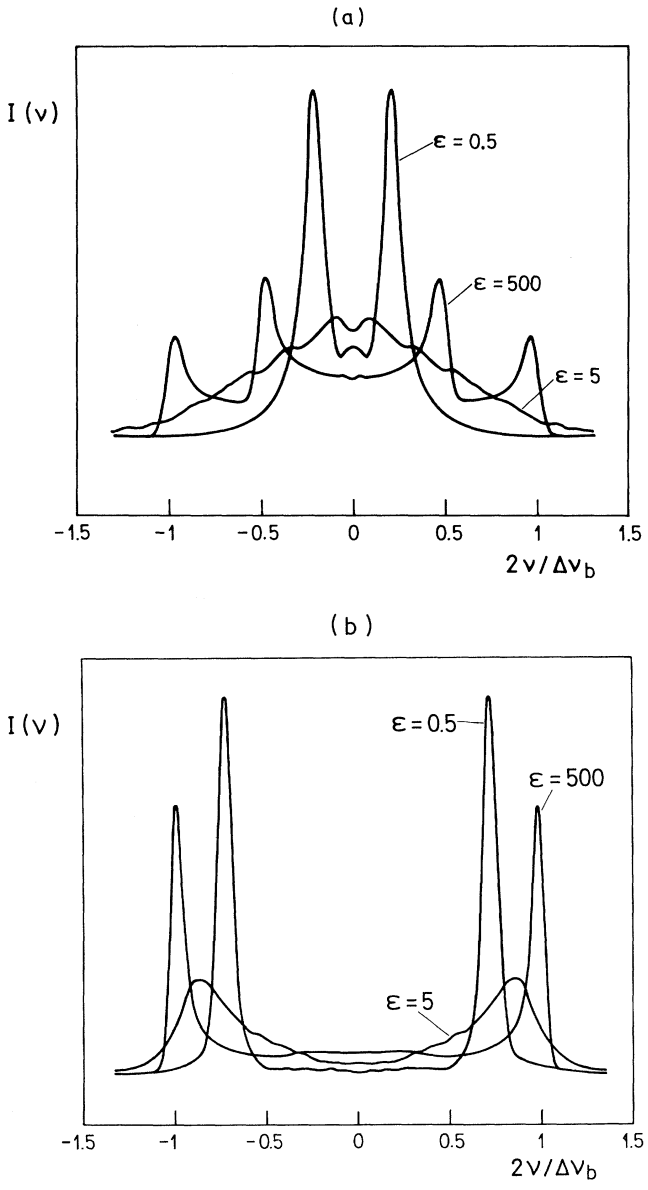

FIG. 4. The effect of translational diffusion on the absorption spectra of the (a) 2D radial-like and (b) 2D axial-like structures presented in Figs. 3(c) and 3(d), respectively.

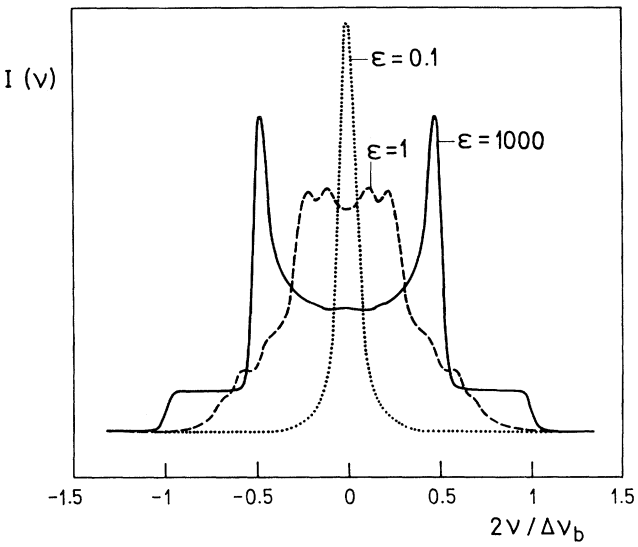

FIG. 5. Numerical simulation of the deuterium NMR spectra of a nematic liquid-crystal spherical droplet with a radial nematic structure for different diffusion rates ϵ.

$I_{cav}(\nu)$ of a droplet with radial structure (stable for $R_{cav} > R_c$) is independent of the orientation of an external magnetic field **B** (assuming it is weak enough) because the director field of this structure is spherically symmetrical. But the absorption spectrum strongly depends on the diffusion rate value ϵ [see Eq. (3) and Fig. 5] due to the relatively strong spatial variation of $\mathbf{n}(\mathbf{r})$.

In the axial structure the director field is predominantly oriented along the average droplet director $\mathbf{N}=\langle \mathbf{n} \rangle_{cav}$, where $\langle\ \rangle_{cav}$ stands for the average over the cavity volume. For all orientations of **B**, the corresponding spectrum $I_{cav}(\nu)$ consists basically of two lines whose separation depends on the angle between **N** and **B**. For the axial structure $I_{cav}(\nu)$ depends relatively weakly on ϵ. With decreasing ϵ the absorption spectrum remains qualitatively the same, only the separation between the two lines is reduced. In the case of 5CB ($K \sim 5\times10^{-12}$ N) and for usual values of surface anchoring strengths, the axial structure is stable in droplets with a radius smaller than 1 μm. In such small droplets the influence of **B** on the director field is negligible [15], and as a consequence, the orientational distribution of **N** is isotropic. In addition, the corresponding ϵ values in this range of cavity radii are smaller than 1 for common D values. Therefore we can assume that the contribution of individual nematic molecules to the absorption spectrum $I_{cav}(\nu)$ of a cavity with an axial structure is averaged over all possible

director orientations within the cavity. The droplet spectrum in this case is the same as that of a homogeneous nematic structure oriented along **N**, but narrower by a factor of $P_2 = \langle 3(\mathbf{n}\cdot\mathbf{N})^2 - 1 \rangle_{cav}/2$. Droplets with an axial structure and the same radius $R_{cav} < 1$ μm would thus give rise to a powder absorption spectrum narrower by a factor of P_2 than the static spectrum of the radial structure.

On the other hand, the NLC droplets of axial structure with different radii R_{cav} give a superposition of the powder spectra $I_{cav}(\nu)$ of various widths since P_2 of an axial structure depends [19] on R_{cav} due to the finite surface-free-energy contribution which is absent in the droplet with radial configuration.

Based on these considerations we can conclude that the absorption spectrum $I(\nu)$ of the whole sample strongly depends on the relative distribution of R_c values, the motional narrowing radius R_ϵ—below which the effect of translational diffusion must be taken into account—and the cavity radius R_{max} corresponding to the maximum of the $P(R_{cav})$ distribution. This is demonstrated in Fig. 6 where $I(\nu)$ is presented for different values of the diffusion constants and R_c, taking into account the distribution $P(R_{cav})$ given in Fig. 1. For such a distribution the resulting spectrum $I(\nu)$ is either (i) Pake powder shaped of width $\Delta\nu_b$ if $R_{max} > R_c$ and $R_{max} > R_\epsilon$ or (ii) composed of Pake powder-shaped contributions of various widths if $R_{max} \geq R_c \geq R_\epsilon$. If $R_{max} \geq R_\epsilon > R_c$ the spectrum gains an additional central line due to an evident contribution from droplets with strongly averaged $I_{cav}(\nu)$.

3. *A note on cavities with tangential anchoring*

In the case of tangential anchoring where the cavity surface tends to orient nematic molecules perpendicular to the surface normal, recent studies of nematic droplets reveal that the bipolar structure [4,15,17,23,24] is commonly stable over the whole anchoring regime. The corresponding absorption spectrum [17] is similar to the one obtained in the axial-like structure. Therefore we believe that in the case of tangential anchoring results would be similar to the homeotropic case assuming that the axial-like structure is stable over the whole anchoring regime.

IV. EXPERIMENTAL RESULTS AND DISCUSSION

The deuterium NMR absorption spectra $I(\nu)$ of the liquid crystal 5CB immersed into the lecithin-treated and nontreated silica aerogel matrices are shown in Fig. 7. The corresponding characteristic width or line-splitting values $\Delta\nu$ of $I(\nu)$ are presented in Fig. 8 compared to the splitting $\Delta\nu_b$ of the bulk NLC.

A. Isotropic phase

The absorption spectra of the 5CB confined in the nontreated aerogel found in the isotropic 5CB phase are wider than in the bulk isotropic phase by a factor ~ 1.5. This is due to the finite local nematic orientational order S_0 within the surface layers, indicating the local ordering tendency of the silica aerogel cavity surfaces. This local ordering persists far into the isotropic phase and is only weakly temperature dependent. Such behavior is expected when the dominant surface interactions are local in nature [25]. The line splitting $\Delta\nu_{iso}$ of the corresponding absorption spectra in the isotropic phase, broadened due to the finite surface ordering effect, can be approximately expressed as [24]

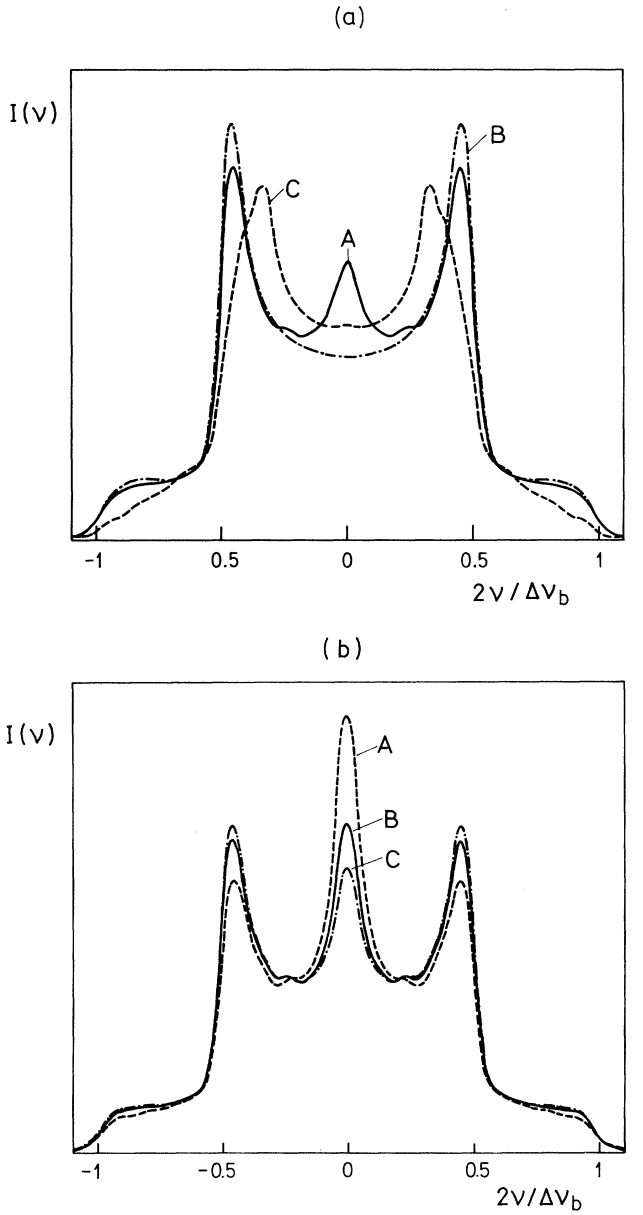

FIG. 6. Numerical simulation of the deuterium NMR spectra of spherical nematic droplets for different values of the diffusion coefficient D and of the critical radius R_c, taking into account the $P(R_{cav})$ distribution presented in Fig. 1. (a) $R_c > 0$ (A: $R_c = 0.01$ μm, $D = 10^{-11}$ m^2 s$^{-1} \rightarrow R_{max} \geq R_\epsilon > R_c$; B: $R_c = 0.01$ μm, $D = 10^{-12}$ m^2 s$^{-1} \rightarrow R_{max} > R_\epsilon$, $R_{max} > R_c$; C: $R_c = 0.1$ μm, $D = 10^{-11}$–10^{-12} m^2 s$^{-1} \rightarrow R_{max} \geq R_c \geq R_\epsilon$). (b) $R_c = 0$ (A: $D = 5\times10^{-11}$ m^2 s^{-1}; B: $D = 10^{-11}$ m^2 s^{-1}; C: $D = 5\times10^{-12}$ m^2 s^{-1}).

$$\Delta\nu_{\rm iso} \sim d(S_0/S_b)\Delta\nu_b \sqrt{(S_0/S_b)\Delta\nu_b \pi/D} \ . \quad (6)$$

In the derivation of this expression it was assumed that S_0 has a constant value within the surface layer of thickness d, and that $d \ll R_{\rm cav}$. For $\Delta\nu_b/S_b \sim 100$ kHz, $d \sim 4$ nm, $D \sim 5\times10^{-12}$ m^2 s^{-1}, and $\Delta\nu_{\rm iso}(W_0) \sim 300$ kHz one finds for a nontreated surface a nearly-temperature-independent local surface order parameter of $S_0 \sim 0.02 \pm 0.01$. For the lecithin-treated sample this value is significantly smaller and cannot be distinguished from the situation in the bulk within the limits of experimental error. This is in contrast with the recent result [25] obtained by deuterium NMR for NLC confined within lecithin-treated cylindrical cavities, where the isotropic surface-induced order was found to be temperature dependent: $S_0 = S_{00}/(2\sqrt{T/T^*-1})$ with $S_{00} = 0.007 \pm 0.001$ and $T^* = T_{NI} - (1.16 \pm 0.05)$ K.

B. Transition region

The experimentally determined absorption spectra of the lecithin-treated sample reveal a discontinuous transition from the isotropic to the nematic phase at $T_{NI} \sim 305$ K. In the case of the nontreated sample the nematic ordering begins to evolve below $T_{NI} \sim 302.5$ K. These T_{NI} values are notably below the bulk transition temperature $T_{NI}^{\rm bulk} \sim 306$ K. In general the shift [8–10] of the transition temperature $\Delta T = T_{NI} - T_{NI}^{\rm bulk}$ can be due to the effects of (i) finite size, (ii) surface interaction strength, (iii) large elastic deformations, and (iv) impurities. ΔT caused by the finite-size effect is of the order of 0.1 K and in our case ($\Delta T > 1$ K) plays a negligible role. The effect of surface interaction can strongly shift T_{NI} ($\Delta T > 0$ for ordering and $\Delta T < 0$ for disordering surfaces) in small cavities ($R_{\rm cav} < 0.1$ μm). If the cavity size is below a critical value $\tilde{R}_c$ the first-order transition between the isotropic and nematic phase even disappears and a continuous change of nematic ordering takes place [2–6]. The value of $\tilde{R}_c$ depends on the cavity shape and the nematic director distribution within it. In a spherical cavity the $\tilde{R}_c$ value lies between [2,4–6,26] 0.067 μm (the bipolar structure) [4] and 0.22 μm (the radial structure) [5]. We believe that in our case this phenomenon plays only a minor role since only 25% (see Fig. 1) of nematic molecules are within cavities of size $R_{\rm cav} < 0.1$ μm. Large elastic deformations can strongly depress T_{NI} only in cavities of size [5] $\sim \tilde{R}_c$. Therefore, the large depression of

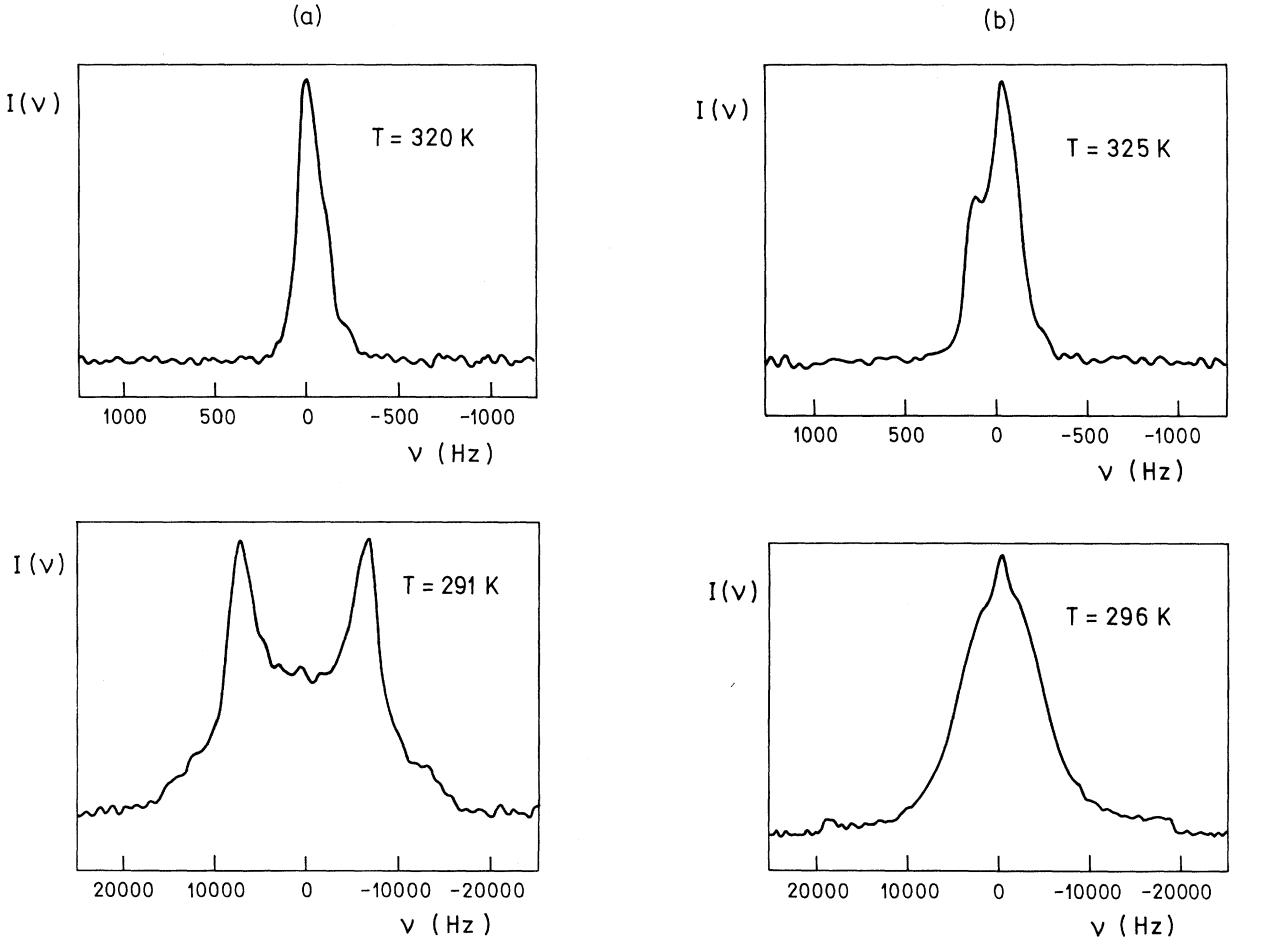

FIG. 7. Experimentally determined deuterium NMR spectra at different temperatures of 5CB in (a) lecithin-treated and (b) nontreated silica aerogel matrices.

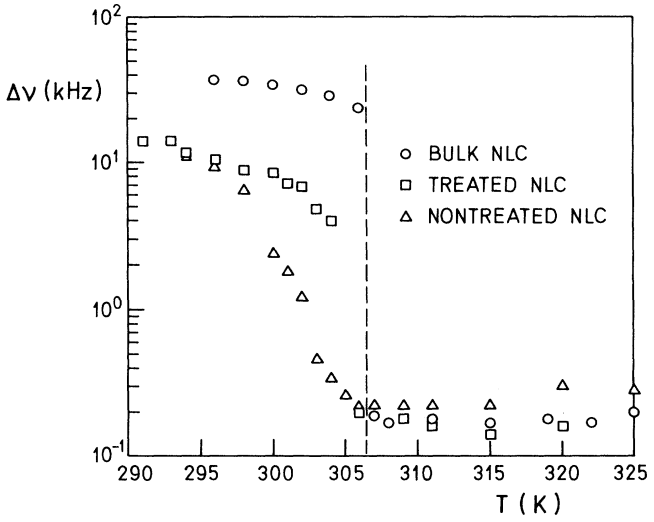

FIG. 8. The half-height $I(\nu)$ width (the isotropic phase, the nematic phase of nontreated sample) or $I(\nu)$ splitting (the nematic phase of the lecithin-treated case) as obtained from the experimentally determined deuterium NMR spectra of 5CB at different temperatures for lecithin-treated and nontreated silica aerogel cavity surfaces. Compare the data with the temperature dependence of the bulk 5CB half-height intensity width data.

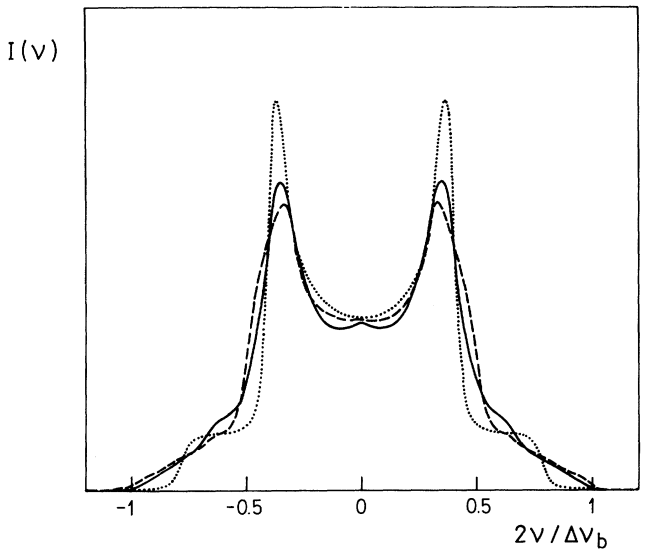

FIG. 9. Comparison of the experimental (full line) and numerically calculated (dashed line) spectrum $I(\nu)$ deep in the nematic phase for the case of the lecithin-treated aerogel surface [$R_c \sim R_\epsilon \sim 1$ μm, $P(R_{cav})$ as given in Fig. 1, and cavities assumed to be spherical]. The static absorption spectrum of a radial structure (dotted line) is shown for comparison.

T_{NI} below T_{NI}^{bulk} ($\Delta T \sim 1$ K for 5CB in the lecithin treated and $\Delta T \sim 4$ K in the nontreated matrix) and the well pronounced first-order-transition character in the case of the lecithin-treated sample (indicating that the majority of the liquid-crystal molecules are in cavities of size $R_{cav} > \tilde{R}_c$) lead to the conclusion that the temperature shifts observed are mostly due to the impurity effect [27]. We also suggest that the impurity effect is more important in the nontreated case (due to different sample preparation) and that the impurity concentration in the nontreated sample strongly varies among the different cavities. This in turn causes a large spread of $T_{NI}^{(cavity)}$ transition temperatures, where in a given cavity a discontinuous nematic-isotropic phase transition occurs.

C. Nematic phase

Let us first analyze the case of 5CB in the lecithin-treated matrix. The experimental results can be simulated by a superposition of Pake powder-shaped spectra of different widths in the case where $R_c \sim R_\epsilon$ (see Fig. 9). This is in accordance with the result obtained for NLC confined to spherical and cylindrical cavities [19,20,22,28], where $\mu_c \sim 10$, corresponding to a critical cavity size [29] of $R_c \sim 1$ μm ($K \sim 5 \times 10^{-12}$ N, $W_0 \sim 3 \times 10^{-5}$ J/m^2 for the lecithin coating), and the diffusion coefficient D between 10^{-11} and 10^{-12} m^2 s^{-1}. The NMR spectra of 5CB in Fig. 7(a) thus strongly support the axial type of nematic director field as presented in the inset of Fig. 3(d).

5CB in the nontreated silica aerogel matrix exhibits a broad central peak with pronounced wings at $\nu \sim \pm \Delta\nu_b$ [see Fig. 7(b)]. These wings are most probably due to the presence of large cavities (see Fig. 1), where the influence of the external field $\mathbf{B}_0$ is dominant ($R_c/\xi \gg 1$) and results in orientation of nematic molecules along the $\mathbf{B}_0$ direction. The broad central peak of $I(\nu)$ can be ascribed to the superposition of absorption spectra $I_R(\nu)$ of different cavities with different nematic ordering due to the spread of T_{NI} values and the enhanced narrow central peak deep in the nematic phase to the motional narrowing effects. This suggests that the structures within cavities are strongly deformed, a situation realized in the case of homeotropic anchoring. The isotropic phase reveals that anchoring in the nontreated sample is much stronger than in the lecithin-treated sample. According to Aliev and Breganov [8,9], the anchoring strength of a nontreated porous glass surface is approximately $W_0 \sim 10^{-3}$ J/m^2. If this estimate is adopted for our case, then $R_\epsilon \sim 1\,\mu\text{m} \gg R_c \sim 0.01$ μm. For the case of spherical droplets we have shown that in this regime a narrow line is added to the spectrum (see Fig. 6).

V. CONCLUSIONS

A deuterium NMR line-shape study of 5CB confined to a silica aerogel of continuous pore structure was performed. Special emphasis was put on the effects of the aerogel surface treatment with lecithin on the temperature evolution of nematic ordering. The absorption spectra of the isotropic phase reveal that the interaction of 5CB with the nontreated aerogel surface is evidently stronger than in the case of the lecithin-treated aerogel surface. The isotropic surface local order parameter for the nontreated aerogel surface is nearly temperature independent and amounts to $S_0 \sim 0.02 \pm 0.01$.

It is quite possible that the nontreated aerogel pores with large values of local order parameters produce a multidomain structure and in fact act as a disordering surface. This is so as the direction of the local ordering may vary in space, so that the pore walls effectively act as pinning impurities. Lecithin treatment, on the other hand, could "smooth" the surfaces out by clogging pores of small radius thus denying access of liquid-crystal molecules into this region. This would diminish contributions of small pores which produce the largest deviations from the ideal powder Pake spectrum.

The above statements agree with the suggestions of Bellini *et al.* [10] that the absence of a discontinuity in the nontreated sample on going from the isotropic to the nematic phase results from the presence of pore walls acting as impurities and thus smearing out the phase-transition singularity similarly as random fields [10,30]. No such smearing out takes place in the lecithin-treated aerogel.

APPENDIX A: EULER-LAGRANGE DIFFERENTIAL EQUATIONS

To obtain the director field within a cavity we solve numerically the Euler-Lagrange differential equations for the director field resulting from the minimization of the Frank free energy [see Eq. (1)] for the case of negligible influence of the external magnetic field.

1. Two-dimensional cavities

In this case the nematic molecules are restricted to the (x,y) plane and the corresponding director field can be presented as $\mathbf{n}=(\cos\theta,\sin\theta)$. Minimization of the free energy leads to the bulk differential equation

$$2\frac{\partial^2\theta}{\partial x^2}(K_{33}\cos^2\theta+K_{11}\sin^2\theta)+2\frac{\partial^2\theta}{\partial y^2}(K_{33}\sin^2\theta+K_{11}\cos^2\theta)$$
$$+(K_{11}-K_{33})\left\{\left[\left[\frac{\partial\theta}{\partial x}\right]^2-\left[\frac{\partial\theta}{\partial y}\right]^2\right]\sin2\theta-2\frac{\partial^2\theta}{\partial x\,\partial y}(\sin2\theta+\cos2\theta)\right\}=0\ .$$

At the cavity boundary strong anchoring is assumed. The boundary (x_s,y_s) is either spherical $(y_s=\pm(R^2-x_s^2)^{1/2},\ x_s\epsilon[-R,R])$ or complementary shaped $(y_s=\pm[R\sqrt{2}-(R^2-x_s^2)^{1/2}],\ x_s\epsilon[-R/\sqrt{2},R/\sqrt{2}];\ y_s=\pm[R^2-(x_s-\sqrt{2}R)^2]^{1/2},\ x_s\epsilon[R(\sqrt{2}-1),R/\sqrt{2}];\ y_s=\pm[R^2-(x_s+\sqrt{2}R)^2]^{1/2},\ x_s\epsilon-[R(\sqrt{2}-1),R/\sqrt{2}])$. Here the index s denotes the cavity boundary.

2. Three-dimensional cavities

In the three-dimensional case we consider only nematic structures within spherical cavities. The director field can be expressed as

$$\mathbf{n}=-(\sin\theta)\mathbf{e}_\vartheta+(\cos\theta)\mathbf{e}_r\ ,$$

where $\mathbf{e}_r$ and $\mathbf{e}_\vartheta$ are unit vectors of the spherical coordinate system and θ the angle between $\mathbf{e}_r$ and $\mathbf{n}$. This ansatz does not take into account structures with twist deformation. The vector field $\mathbf{n}$ is in this case completely described by a scalar field $\theta(r,\vartheta)$, which satisfies the bulk differential equation

$$(K_{11}\sin^2\theta+K_{33}\cos^2\theta)\left[\frac{\partial^2\theta}{\partial r^2}r^2+2\frac{\partial\theta}{\partial r}r\right]+(K_{11}\cos^2\theta+K_{33}\sin^2\theta)\left[\frac{\partial^2\theta}{\partial\vartheta^2}+\frac{\partial\theta}{\partial\vartheta}\cot\vartheta\right]$$
$$-K_{11}\frac{\sin2\theta}{2}(\cot^2\vartheta-1)+(K_{11}+K_{33})\cot\vartheta\sin^2\theta$$
$$+\frac{(K_{11}-K_{33})}{2}\left\{\sin2\theta\left[r^2\left[\frac{\partial\theta}{\partial r}\right]^2+r\frac{\partial\theta}{\partial r}\cot\vartheta-\left[\frac{\partial\theta}{\partial\vartheta}\right]^2+\frac{\partial\theta}{\partial\vartheta}+2r\frac{\partial^2\theta}{\partial r\,\partial\vartheta}\right]+2\cos(2\theta)\frac{\partial\theta\,\partial\theta}{\partial\vartheta\,\partial r}r\right\}=0\ .$$

In this case we take into account weak anchoring at the droplet surface which yields an additional differential equation serving as boundary condition (at $r=R$):

$$\left[r\frac{\partial\theta}{\partial r}[\sin^2\theta+(K_{33}/K_{11})\cos^2\theta]\right.$$
$$+\frac{\partial\theta}{\partial\vartheta}(1-K_{33}/K_{11})\sin\theta\cos\theta$$
$$-\cos\theta\sin\theta(2-K_{33}/K_{11})$$
$$\left.+\cot\vartheta\sin^2\theta+\mu\cos\theta\sin\theta\right]=0\ .$$

APPENDIX B: EVALUATION OF $G(t)$

To evaluate numerically the autocorrelation function $G(t)$ [defined in Eq. (4b)] for a given nematic configuration within a cavity we use the isotropic random-jump diffusion model. Within this model the translational diffusion of nematic molecules is simulated with random jumps over points of a two- or three-dimensional (depending on the 2D or 3D model) square lattice of a lattice constant a. The value of a is chosen small enough so that the director field far from point defects is only slightly altered when a nematic molecule is displaced for a distance a. At the cavity boundary a

reflection of nematic molecules is assumed. Further we neglect the anisotropy of the diffusion tensor and let the nematic molecules jump only on the nearest lattice sites. The jump time is given by $\tau = a^2/6D$. According to this model $G(t)$ can be expressed as [15,17]

$$G(t=n\cdot\tau)=\langle \exp\{i2\pi[\Delta\nu(\mathbf{r}_{j1}^{(k)})+\Delta\nu(\mathbf{r}_{j2}^{(k)}) + \cdots +\Delta\nu(\mathbf{r}_{jn}^{(k)})]\tau\}\rangle_{j,k} .$$

Here $\Delta\nu(\mathbf{r}_{jl}^{(k)})$ denotes the deuterium line splitting [see Eq. (2)] of a nematic molecule positioned at $\mathbf{r}_{jl}^{(k)}$, where the index l describes a position of a nematic molecule after l jumps on the kth path originating from the initial position, described with index j. The ensemble average in Eq. (4b) is in our calculations approximated with an average $\langle\ \rangle_{j,k}$ over different initial points j and paths k leading from these points.

The resulting spectrum is afterwards broadened by convolution with a Gaussian line shape of width $\delta\nu$.

[1] P. Sheng, Phys. Rev. Lett. **37**, 1059 (1976).
[2] P. Sheng, Phys. Rev. A **26**, 1610 (1982).
[3] A. Poniewierski and T. J. Sluckin, Liq. Cryst. **2**, 281 (1987).
[4] I. Vilfan, M. Vilfan, and S. Žumer, Phys. Rev. A **40**, 4724 (1990).
[5] S. Kralj, S. Žumer, and D. W. Allender, Phys. Rev. A **34**, 2943 (1991).
[6] P. G. Ferreira and M. M. Telo da Gama, Physica A **179**, 179 (1991).
[7] R. M. A. Hikmet and B. H. Zwerver, Liq. Cryst. **12**, 319 (1992).
[8] F. M. Aliev, Kristallografiya **33**, 969 (1988) [Sov. Phys. Crystallogr. **33**, 573 (1988)].
[9] F. M. Aliev and M. N. Breganov, Zh. Eksp. Teor. Fiz. **95**, 122 (1989) [Sov. Phys.—JETP **68**, 70 (1989)].
[10] T. Bellini, N. A. Clark, C. D. Muzny, L. Wu, C. W. Garland, D. W. Schaefer, and B. J. Oliver, Phys. Rev. Lett. **69**, 788 (1992).
[11] J. Fricke, J. Non-Cryst. Solids **100**, 169 (1988).
[12] A. Abragam, *The Principles of Nuclear Magnetism* (Clarendon, Oxford, 1962).
[13] P. G. de Gennes, *The Physics of Liquid Crystals* (Clarendon, Oxford, 1974).
[14] M. Chaput (private communication).
[15] A. Golemme, S. Žumer, D. W. Allender, and J. W. Doane, Phys. Rev. Lett. **61**, 2937 (1988).
[16] S. Žumer, S. Kralj, and M. Vilfan, J. Chem. Phys. **91**, 6411 (1989).
[17] S. Kralj, M. Vilfan, and S. Žumer, Liq. Cryst. **5**, 1489 (1989).
[18] F. Simoni, F. M. Aliev, F. Basile, F. Bloisi, and L. Vicari, in *The 14th International Liquid Crystal Conference, Abstracts,* Proceedings of the 14th International Liquid Crystal Conference, Pisa, 1992, edited by E. Chiellini (Taylor & Francis, London, 1992), p. 327.
[19] S. Kralj and S. Žumer, Phys. Rev. A **45**, 2461 (1992).
[20] S. Kralj and S. Žumer (unpublished).
[21] I. Vilfan, M. Vilfan, and S. Žumer, Phys. Rev. A **43**, 6875 (1991).
[22] J. H. Erdmann, S. Žumer, and J. W. Doane, Phys. Rev. Lett. **64**, 19 (1990).
[23] S. Žumer, and J. W. Doane, Phys. Rev. A **34**, 3373 (1986).
[24] J. Dolinšek, O. Jarh, M. Vilfan, S. Žumer, R. Blinc, J. W. Doane, and G. P. Crawford, J. Chem. Phys. **95**, 2154 (1991).
[25] G. P. Crawford, R. Stannarius, and J. W. Doane, Phys. Rev. A **44**, 2558 (1991).
[26] A. Golemme, S. Žumer, J. W. Doane, and M. E. Neubert, Phys. Rev. A **37**, 559 (1988).
[27] G. R. Alms, T. D. Gierke, and W. H. Flygare, J. Chem. Phys. **61**, 4083 (1974).
[28] D. W. Allender, G. P. Crawford, and J. W. Doane, Phys. Rev. Lett. **67**, 1442 (1991).
[29] G. P. Crawford, R. O. Crawford, S. Žumer, and J. W. Doane, in *The 14th International Liquid Crystal Conference, Abstracts* (Ref. [18]), p. 375.
[30] A. Maritan, M. R. Swift, M. Cieplak, M. H. W. Chan, M. W. Cole, and J. R. Banavar, Phys. Rev. Lett. **67**, 1821 (1991).

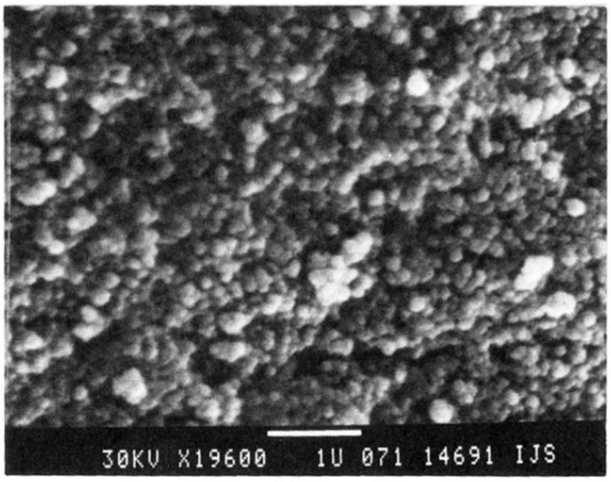

FIG. 2. Scanning electron micrograph of the silica aerogel matrix.